Corrosion Science xxx (2013) xxx–xxx

Contents lists available at SciVerse ScienceDirect

Corrosion Science

journal homepage: www.elsevier.com/locate/corsci

Effect of the anionic part of various Ce(III) salts on the corrosion inhibition efficiency of AA2024 aluminium alloy

M. Machkova [a], E.A. Matter [b,*], S. Kozhukharov [a], V. Kozhukharov [a]

[a] University of Chemical Technology and Metallurgy, 8 Kl. Ohridski, 1756 Sofia, Bulgaria
[b] Department of Chemistry, Faculty of Science, Damanhour University, 22111 Damanhour, Egypt

ARTICLE INFO

Article history:
Received 12 July 2012
Accepted 2 January 2013
Available online xxxx

Keywords:
A. Alloy
A. Rare earth elements
B. EIS
B. SEM
C. Neutral inhibition

ABSTRACT

Systematic investigations on the inhibitive efficiency of different Ce(III) salts against the corrosion of AA2024 in 0.01 M NaCl are performed. Various concentrations (from 10^{-5} to 10^{-2} M) for each Ce-salt are investigated after different exposure periods up to 600 h. Their inhibitive abilities were evaluated by: Linear Sweep Voltammetry (LSV) and Electrochemical Impedance Spectroscopy (EIS) combined with SEM observation and EDX analysis. A strong influence of the Ce-salts anionic parts on the inhibitive efficiencies and the mechanism of the protective behaviour are found. The inhibitive efficiencies of the Ce(III) salts are ordered as: $Ce(NO_3)_3 > (NH_4)_2Ce(NO_3)_5 > Ce_2(SO_4)_3 > CeCl_3$.

1. Introduction

Because of their remarkable strength and mechanical resistivity, combined with relatively low weight and low prices, the aluminium alloys have found a wide spread applications in various household and technique fields. Regarding their popularity these alloys follow immediately the steels and the cast iron. But they possess low corrosion resistivity. Cu, Mg, Si, Fe, Mn, etc. used as alloying elements form intermetallic phases dispersed in the alloys' bulk. They render the mechanical stability and resistivity to the Al-alloys but become centres of initiation and further propagation of localised corrosion when the latter are in contact with media containing Cl^- ions. That is why the alloys require an appropriate corrosion protection prior to application. The experience has shown that Cr(VI) species appear to be excellent inhibitors of the corrosion of aluminium and some other alloys [1–4]. Due to their toxic character and carcinogenic activity their usage has already been banned in many countries. Numerous organic [5–11] and inorganic compounds are tested [12–14] with the aim to discover an environmentally friendly alternative of the chromates. The rare-earth elements, some of which are widely spread in nature, have proven to be the most perspective inhibitors of Al-corrosion.

The pioneer works on the employment of rare-earth salts as inhibitors of aluminium corrosion belong to Hinton et al. [15,16]. The latter have investigated the protective activity of $CeCl_3$ against uniform and pitting corrosion of zinc containing AA7075 aluminium alloy. Similar investigations on other compounds of rare-earth elements [17–21] and other aluminium alloys [22–24] have been also undertaken. Reliable results have been achieved when cerium compounds, such as chlorides [22,24], nitrates [25–27], sulphates [28], and even some double Ce-salts [29,30] have been used. The attention in these investigations has been mainly focused on the role of the cerium cation on the corrosion inhibitive ability while the effect of the respective anions has not been taken into an account. A few investigations report that the counter ions of some cerium salt can reveal some influence. It is found [27] that the cerium ions inhibitive effect is masked by the presence of oxygen containing anions when $Ce(NO_3)_3$ or $Ce_2(SO_4)_3$ is used. There are data concerning the influence of the anionic compositional part of various Ce(III) salts on the characteristics of Ce-conversion coatings deposited on AZ31 [31]. Similar investigations are reported for AA6082 aluminium alloy [32] as well. The authors have established that the best coatings are obtained in solutions of $CeCl_3$, whereas these of $Ce_2(SO_4)_3$ have revealed the worst results. It is also mentioned there that the mechanism of the nitrate ions action remains unclear.

However, no thorough investigation regarding the influence of the anionic compositional part of Ce-salts on their inhibitive efficiency is found in the literature. The aim of this paper is to report results obtained in systematic comparative investigations evaluating the inhibitive ability of various cerium salts in their third oxidation state ($CeCl_3$, $Ce_2(SO_4)_3$, $Ce(NO_3)_3$ and $(NH_4)_2Ce(NO_3)_5$) against the corrosion of AA2024 aluminium alloy in 0.01 M NaCl solution.

* Corresponding author. Tel.: +20 102383394; fax: +20 482776043.
E-mail address: e_a_matter@yahoo.com (E.A. Matter).

0010-938X/$ - see front matter © 2013 Elsevier Ltd. All rights reserved.
http://dx.doi.org/10.1016/j.corsci.2013.01.008

2. Experimental

2.1. Chemical composition, preliminary treatment of specimens and solution preparation

The exact composition of the AA2024 alloy presented in Table 1 was analysed by inductively coupled plasma–optical emission spectroscopy (ICP–OES) after dissolution of the alloy in an acidic medium.

All AA2024 specimens investigated were preliminary abraded by SiC emery papers (starting with paper of 220 grit size, going through that of 360 and 500 and finishing with paper of 800 grit size). Then they were degreased for 10 min in ethanol:ether (1:1) mixture, and rinsed vigorously with tap and then with distilled water. Finally, they were exposed to the corrosive medium in absence and in presence of an inhibitor.

Aqueous solutions of 0.01 M NaCl containing different amounts (from 1×10^{-5} M to 1×10^{-2} M) of the cerium (III) salts were used as model corrosive media. All cerium salts were products of Alfa Aesar (Karlsruhe, Germany): 99.00% purity grade $CeCl_3 \cdot 7H_2O$, 99.00% purity grade $Ce(NO_3)_3 \cdot 7H_2O$, 99.99% purity grade $Ce_2(SO_4)_3 \cdot 8H_2O$ and reagent grade $(NH_4)_2Ce(NO_3)_5 \cdot 4H_2O$.

2.2. Equipment and methods of measurement

2.2.1. Electrochemical measurements

The electrochemical measurements were performed in a 100 ml flat three-electrode cell. Limited zones of the metallic plates of an area of 2.0 cm^2 exposed to the corrosive medium served as working electrodes. A platinum net cylinder was used as a counter electrode. Its surface area was two orders of magnitude higher than that of the working electrode. A commercial Ag/AgCl 3 M KCl electrode (model 6.0733.100, product of Metrohm) was used as a reference electrode. Its potential value is 0.2098 V in respect to standard hydrogen electrode, SHE, and is referred further in the text as SSC.

The polarisation curves were recorded by a potentiostat/galvanostat AUTOLAB PG 30/2 of ECOCHEMIE (Netherlands) supported by a frequency response analyzer FRA-2. A Faraday cage was used in order to avoid external electromagnetic and electrostatic discharges influence on the electrochemical cell. All measurements were carried out at room temperature.

The establishment of a constant value of the open circuit potential, *OCP*, is aimed. The *OCP* – *t* dependences obtained in distilled water, 0.01 M NaCl, and cerium containing 0.01 M NaCl solution are presented in Fig. 1

It shows that the curve has an identical form in the three media chosen. The potential increases with the time increase, reaches a maximum and then decreases to a constant value. This potential change with time is attributed to oxide layer formation upon the immersion of the respective sample in the corrosive medium and the simultaneously proceeding attack by the chloride ions contained in the solution. The *OCP* – *t* curves obtained show that stable and reliable results can be obtained after at least 8–10 h of exposure to the respective solutions. To exclude the influence of the working electrode polarisation accurately, all the electrochemical measurements were performed after 24 h of samples exposition to the corrosive medium.

The polarisation curves were recorded in a narrow interval around the open circuit potential (*OCP* ± 0.03 V) at a scan rate of 1 mV/s. In case of lower scan rate application well expressed current deviations were registered, which did not provide the accurate determination of the corrosion potential, E_{corr}, and the polarisation resistance, R_p. Afterwards the respective impedance spectra were recorded. This was done in the frequency range from 10^4 to 10^{-2} Hz distributed in 7 frequencies per decade with signal amplitude of 10 mV in respect to *OCP*. The acquisition of the impedance spectra was followed by cathodic polarisation curves recording in the range from *OCP* + 30 mV to *OCP* - 500 mV at a scan rate of 1 mV/s. Finally after retaining the *OCP* value, anodic polarisation curves are recorded in the range from *OCP* - 30 mV up to *OCP* + 700 mV at a scan rate of 1 mV/s. This experimental sequence enabled the achievement of high correspondence between E_{corr} determined by the polarisation curves and *OCP* measured prior to the performance of the polarisation measurements. The values of the polarisation resistance R_p were estimated as an average result of at least three identical measurements on individual electrodes.

Table 1
Composition of the aluminium alloy investigated determined by ICP – OES.

Element	Cu	Fe	Mg	Mn	Ni	Si	Al
Content (wt.%)	3.716	0.404	1.259	0.537	0.055	<0.01	balance

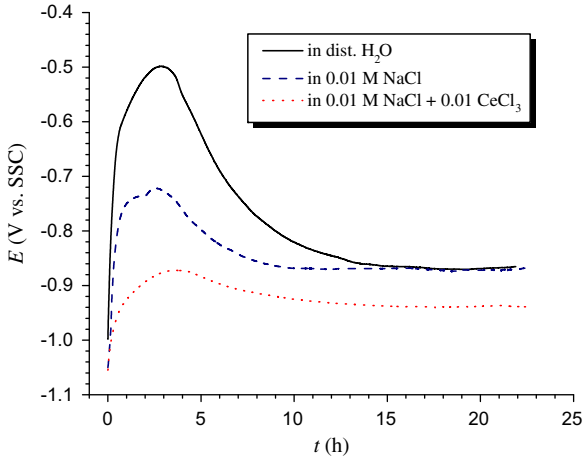

Fig. 1. Evolution of *OCP* within the exposition time for AA2024 samples immersed in different media.

2.2.2. Morphological characterisations

SEM images were recorded using scanning electron microscopy (TESCAN, SEM/FIB LYRA I XMU). The local composition was studied using energy dispersion X-ray spectroscopy, EDX (Quantax 200 of BRUKER detector) connected to the SEM-device.

3. Results and discussion

3.1. Polarisation measurements

The discussion of the experimental results is done on the basis of the concepts of AA2024 aluminium alloy pitting corrosion and the inhibitive action of Ce(III) ions.

The intermetallic inclusions of the S-phase (Al_2CuMg) are responsible for the local corrosion of the Al-alloy. As precipitated particles these inclusions occupy a 3% of the entire metal surface. In neutral or weakly acidic media containing Cl^- ions, Mg and Al from these particles undergo chemical [22] or electrochemical [33] dissolution. This results in the particles copper enrichment. Hence, they become microcathodes where the conjugated partial reaction of oxygen reduction occurs:

$$O_2 + 2H_2O + 4e^- \rightarrow 4OH^- \quad (1)$$

This reaction brings about pH increase which in turn favours the dissolution of the oxide layer and the aluminium matrix around the particles, i.e. the following reactions [33] start to proceed:

$$Al_2O_3 + 2OH^-_{(ads)} \rightarrow 2AlO_2^- + H_2O \quad (2)$$

Please cite this article in press as: M. Machkova et al., Effect of the anionic part of various Ce(III) salts on the corrosion inhibition efficiency of AA2024 aluminium alloy, Corros. Sci. (2013), http://dx.doi.org/10.1016/j.corsci.2013.01.008

$$2Al_{(metallic)} + 3H_2O \rightarrow Al_2O_3 + 3H_2 \uparrow \quad (3)$$

Due to reaction (1) almost insoluble Ce oxides and hydroxides appear at the cathodic areas in presence of cerium salts:

$$Ce^{3+} + 2OH^- \rightarrow Ce(OH)_2^+ \quad (4)$$

$$Ce^{3+} + 3OH^- \rightarrow Ce(OH)_3 \downarrow \quad (5)$$

They create a barrier between the actively decomposing S-phase particles (corrosion pits) and the surrounding corrosive medium hindering thus the entire corrosion process.

Fig. 2 shows cathodic polarisation curves recorded on alloy samples after 24 h of exposition to the model corrosive media containing 5×10^{-5} M (a) and 1×10^{-2} M (b) concentration of different cerium salts.

It is seen that the corrosion potentials of the specimens exposed to solutions of different Ce-salts differ from that of the referent solution (0.01 M NaCl). These differences outline better with the increase of corresponding cerium salt concentration. Fig. 2b shows also that E_{corr} recorded in $CeCl_3$ containing solution shifts by 100 mV towards more negative values when referred to that of the electrode exposed to the referent corrosive medium. There is a shift of E_{corr} but in positive direction in solutions of cerium salts of oxygen containing acids. This fact is indicative of a difference in the mechanism of the inhibitive action of the cerium salts investigated.

The current densities of polarisation curves depend also on the anionic compositional part of the cerium salts studied. At lower concentrations (5×10^{-5} M) the polarisation curves obtained in solutions of different cerium salts almost coincide with the referent one in the higher potential range. It looks as if the Ce(III) salts have almost no effect on the corrosion process. This result can be explained by the assumption that the deposition of cerium hydroxides of clearly expressed characteristics is a relatively slow process [34]. Therefore, only some of the cathodic zones on the metallic surface are covered by Ce-deposits after the initial 24 h of exposition, while the majority of them having lower activity remain uncovered. That is the reason for the almost identical rates of the corrosion processes in absence and in presence of any Ce-salt at low concentration.

At a higher concentration of the inhibitors (1×10^{-2} M) in fact all cathodic zones are already covered by Ce-deposits after the initial 24 h of exposition. This results in a significant change of E_{corr} and the corrosion rate. They differ substantially from those found in the referent NaCl solution as shown in Fig. 2b.

Fig. 2b reveals also that at a definite potential value the cathodic current densities have values different from that of the referent curve. For instance, in the case of $(NH_4)_2Ce(NO_3)_5$ the current density at E = 1.1 V is an order of magnitude higher than that of the referent one. The cathodic current densities recorded in presence of $Ce(NO_3)_3$ are even higher. A question arises: is it possible to observe inhibition of the entire corrosion process by $(NH_4)_2Ce(NO_3)_5$ and $Ce(NO_3)_3$ irrespectively of the fact that the higher cathodic current densities indicate enhancement of the cathodic conjugated partial reaction? Looking for the answer a phenomenon typical for metals with aptitude to form superficial oxide films is considered. It is found that depending on the concentration some oxidizers act simultaneously as accelerators of the cathodic partial reaction and as inhibitors of the anodic dissolution of the metal [35]. To verify that this is the mechanism of the inhibitive action of $(NH_4)_2Ce(NO_3)_5$ and $Ce(NO_3)_3$ one has to compare the shape of the anodic and the respective cathodic polarisation curves recorded under identical conditions. Fig. 3 shows anodic polarisation curves of AA2024 samples after 24 h of exposition to 0.01 M NaCl model corrosive medium containing 5×10^{-5} M (a) and 1×10^{-2} M (b) of Ce-salts.

It is seen from Fig. 3 that at very low concentrations (Fig. 3a) the anodic polarisation curves obtained in presence of the cerium salts discussed have a form similar to that of the referent curve. In all these curves two sharp increases of the anodic current densities at definite potential values are outlined. One of these appears at E_{corr} and is related to the dissolution of the S-phase intermetallics, whereas the other one is observed at the pitting nucleation potential, E_{pit}, and corresponds to the dissolution processes at the intergranular boundaries in the matrix crystals [36]. It is worth noting that the anodic current densities in the range between E_{corr} and E_{pit} are different for the Ce-salts studied. This difference is even better expressed in case of higher concentrations (Fig. 3b). It is seen that the curves recorded in solutions containing $(NH_4)_2Ce(NO_3)_5$ and $Ce(NO_3)_3$ are almost horizontal which can be accepted as indicative of the absence of any intergranular corrosion at the crystal boundaries in the basic Al-matrix. Besides, E_{corr} is strongly shifted in anodic direction when compared to E_{corr} of the referent curve. The facts considered as well as the corresponding cathodic polarisation curves show that $(NH_4)_2Ce(NO_3)_5$ and $Ce(NO_3)_3$ act as depolarisers, similarly to the oxygen dissolved in the electrolyte. On the other hand, due to the copper re-deposition as a result of the corrosion of the intermetallic particles [34] and the basic Al–matrix [14], the total cathodic area becomes larger than the anodic one. These copper re-deposits provide an additional area for the cathodic processes [37]. Oxygen reduction can take place on these copper re-deposits which leads to Cu_2O film formation. It passivates their surface and hinders further oxygen reduction. The film considered cannot appear in presence of NO_3^- ions in the electrolyte solution because of the following reaction [38]:

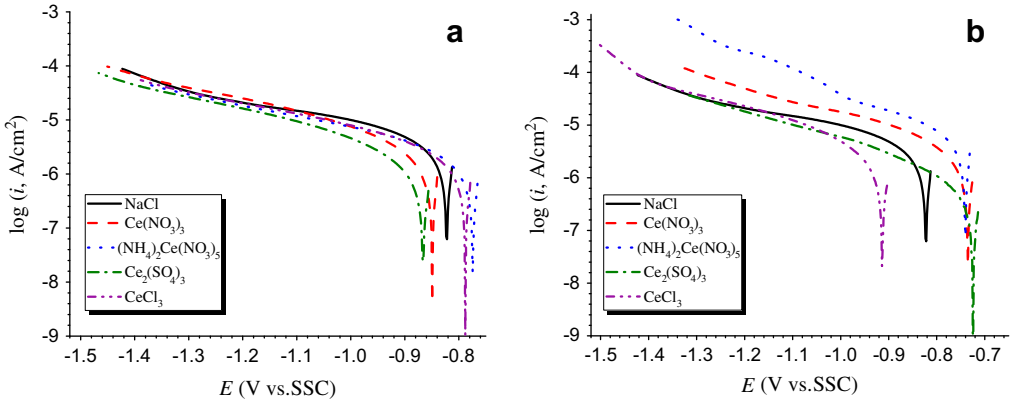

Fig. 2. Cathodic polarisation curves of AA2024 specimens after 24 h of exposure into 0.01 M NaCl solutions without and with: (a) 5×10^{-5} M and (b) 1×10^{-2} M concentration of the respective Ce(III) salts.

Please cite this article in press as: M. Machkova et al., Effect of the anionic part of various Ce(III) salts on the corrosion inhibition efficiency of AA2024 aluminium alloy, Corros. Sci. (2013), http://dx.doi.org/10.1016/j.corsci.2013.01.008

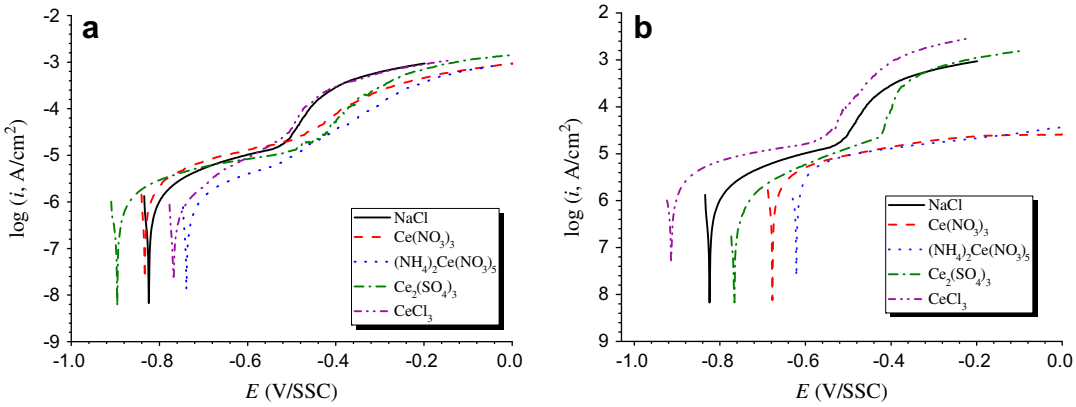

Fig. 3. Anodic polarisation curves of AA2024 specimens, after 24 h of exposure into 0.01 M NaCl solutions without and with (a) 5×10^{-5} M and (b) 1×10^{-2} M concentration of the respective Ce(III) salts.

$$3Cu_2O + 14H^+ + 2NO_3^- \rightarrow 6Cu^{2+} + 2NO + 7H_2O \quad (6)$$

The NO_3^- anions present in the electrolyte dissolve the superficial copper oxide film to keep the copper surface uncovered and hence available to a continuous oxygen reduction proceeding. That is the reason for the registration of higher current values in the cathodic polarisation curves recorded in presence of $(NH_4)_2Ce(NO_3)_5$ and $Ce(NO_3)_3$ when compared to those of the referent one (Fig. 2b). As the copper re-deposits occupy a significant fraction of the surface, the cathodic current density is very low and causes a negligible shift of E_{corr} in cathodic direction. The area occupied by the anodic zones is small and consequently the anodic corrosion current density is much higher than the cathodic one. It is high enough to cause a significant shift of E_{corr} in anodic direction. The potential of the anodic zones can reach values that enable anodic oxide film formation and hence electrode passivation, i.e. the control of the corrosion process becomes an anodic one.

The polarisation curves in Figs. 2 and 3 illustrate in a qualitative form the difference in the corrosion behaviour of the alloy samples after 24 h of exposure to solutions of 0.01 M NaCl containing different Ce(III) salts. The quantitative determination of the inhibitive efficiency of the Ce salts studied requires the determination of the polarisation resistance, R_p, average values. They are estimated on the ground of polarisation curves recorded in a narrow interval around the *OCP* value (*OCP* +/−0.030 V). The R_p values obtained provide the determination of the coefficient of protective ability, γ, and the inhibition efficiency, η, in accordance with Eqs. (7) and (8), respectively:

$$\gamma = \frac{R_p^{inh}}{R_p^0} \quad (7)$$

$$\eta(\%) = \left(1 - \frac{R_p^0}{R_p^{inh}}\right) \times 100 \quad (8)$$

where R_p^0 is the polarisation resistance determined in the referent solution, while R_p^{inh} is the polarisation resistance measured in each Ce-inhibitor containing solution.

Compared to η, the coefficient γ expresses better the inhibitive activities differences and which is why is more relevant as a basis for comparison. The values of γ and η are found for all Ce-salts investigated in concentration of 1×10^{-3} M and 5×10^{-5} M for exposure time ranging from 24 to 600 h.

Tables 2a and 2b present the values of R_p, γ and η in case of exposure of the specimens studied to 0.01 M NaCl model corrosive media containing 1×10^{-3} M of different Ce-inhibitors. Tables 3a and 3b show the respective values obtained for 5×10^{-5} M presence of the salts investigated. The average values shown in both tables are obtained on the ground of at least three measurements on individual AA2024 specimens.

The data in Table 2b reveal that η increases constantly during the entire exposition of the samples to the corrosive media. This fact can be explained assuming that the cathodic areas exhibit different activities [39]. The less active cathodic areas are even additionally suppressed in presence of the more active ones. When the latter areas are already suppressed by the Ce-hydroxide deposits, the less active cathodes become the main cathodic centres. Supplemental quantities of Ce-hydroxide deposits on these locations lead to further increase of γ and the total resistance at the metal/electrolyte interface. The data in Table 2 show also that γ values of the respective cerium salts are influenced by their anionic part.

For AA2024 specimens exposure time between 144 and 600 h, the cerium (III) salts can be conditionally divided into two groups in respect to their inhibitive efficiency: (i) more efficient with γ ranging from 27 to 39, and (ii) less efficient with γ ranging from 5 to 16. The higher efficiencies of $(NH_4)_2Ce(NO_3)_5$ and $Ce(NO_3)_3$ result from the presence of NO_3^- group, which as mentioned above, influences the inhibition mechanism. During the initial hours of exposition (up to 72 h), $Ce_2(SO_4)_3$ appears to be the most efficient inhibitor among all Ce(III) salts investigated. This phenomenon can be explained by the fact that the sulphate anions suffer preferable adsorption when compared to Cl^- ions [40] and the formation of a salt film on the electrode surface becomes possible. It reveals a weak additional protective activity hindering the aggressive Cl^- ions access to the surface.

The data in Tables 3a and 3b show that the influence of the Ce-salts anionic compositional part becomes indistinguishable at lower concentrations (5×10^{-5} M). After 24 h of exposure the γ values of the respective Ce-salts vary in a very narrow range from 4.02 to 4.98. Notable differences of the γ values arise after more extended times of exposure. The comparison of the data in Tables 2 and 3

Table 2a
Average values of the polarisation resistance with their standard deviation ($R_p \pm S$) obtained for AA2024 samples after different periods of exposition into 0.01 M NaCl containing 1×10^{-3} M concentration of different Ce-salts.

Time (h)	$(R_p \pm S) \times 10^4$ (Ω cm^2)			
	$Ce(NO_3)_3$	$(NH_4)_2Ce(NO_3)_5$	$Ce_2(SO_4)_3$	$CeCl_3$
24	14.2 ± 1.2	6.60 ± 0.56	20.7 ± 1.6	5.10 ± 0.56
72	21.8 ± 1.95	13.4 ± 1.1	18.3 ± 1.3	6.00 ± 0.52
144	29.3 ± 2.51	17.9 ± 1.3	13.7 ± 1.0	6.60 ± 0.61
240	36.8 ± 3.31	31.6 ± 3.6	16.7 ± 1.2	9.70 ± 0.77
360	39.4 ± 3.6	33.8 ± 3.6	17.4 ± 1.3	10.7 ± 1.21
480	43.1 ± 4.7	35.6 ± 3.9	17.6 ± 1.3	18.3 ± 1.5
600	46.4 ± 4.8	43.2 ± 4.6	19.35 ± 1.5	29.7 ± 2.3

Please cite this article in press as: M. Machkova et al., Effect of the anionic part of various Ce(III) salts on the corrosion inhibition efficiency of AA2024 aluminium alloy, Corros. Sci. (2013), http://dx.doi.org/10.1016/j.corsci.2013.01.008

Table 2b
Inhibition efficiency η (%) and the coefficient of protective ability γ, obtained for AA2024 samples after different periods of immersion in 0.01 M NaCl containing 1×10^{-3} M concentration of different Ce-salts.

Time (h)	$Ce(NO_3)_3$		$(NH_4)_2Ce(NO_3)_5$		$Ce_2(SO_4)_3$		$CeCl_3$	
	η	γ	η	γ	η	γ	η	γ
24	91.7	12.0	82.3	5.6	94.3	17.7	77.1	4.4
72	94.6	18.6	91.3	11.5	93.6	15.6	80.5	5.1
144	96.0	25.0	93.5	15.3	91.5	11.7	82.3	5.6
240	96.8	31.5	96.3	27.4	93.0	14.3	87.9	8.3
360	97.0	33.7	96.5	28.9	93.3	14.9	89.1	9.1
480	97.3	36.8	96.7	30.4	93.4	15.0	93.6	15.6
600	97.5	39.7	97.3	37.0	93.9	16.5	95.9	25.4

Table 3a
Average values of the polarisation resistance with their standard deviation ($R_p \pm S$) obtained for AA2024 samples after different periods of exposition into 0.01 M NaCl containing 5×10^{-5} M concentration of different Ce-salts.

Time (h)	$(R_p \pm S) \times 10^4$ (Ω cm^2)			
	$Ce(NO_3)_3$	$(NH_4)_2Ce(NO_3)_5$	$Ce_2(SO_4)_3$	$CeCl_3$
24	5.83 ± 0.67	5.38 ± 0.58	4.70 ± 0.51	5.53 ± 0.63
72	8.82 ± 0.95	7.46 ± 0.82	8.33 ± 0.78	6.20 ± 0.70
144	18.9 ± 1.62	13.5 ± 1.1	10.7 ± 1.2	7.37 ± 0.81
240	22.9 ± 1.71	20.2 ± 1.9	14.2 ± 1.1	9.24 ± 0.76
360	30.3 ± 3.1	27.7 ± 2.5	15.2 ± 1.3	10.4 ± 0.91
480	31.6 ± 3.4	30.9 ± 3.2	17.4 ± 1.6	12.5 ± 1.1
600	45.8 ± 5.2	42.7 ± 4.9	18.7 ± 1.6	–

Table 3b
Inhibition efficiency η (%) and the coefficient of protective ability γ, obtained for AA2024 samples after different periods of immersion in 0.01 M NaCl containing 5×10^{-5} M concentration of different Ce-salts.

Time (h)	$Ce(NO_3)_3$		$(NH_4)_2Ce(NO_3)_5$		$Ce_2(SO_4)_3$		$CeCl_3$	
	η	γ	η	γ	η	γ	η	γ
24	80.0	4.98	78.3	4.60	75.1	4.02	78.8	4.73
72	86.7	7.54	84.3	6.37	86.0	7.12	81.0	5.30
144	93.8	16.2	91.0	11.5	89.1	9.14	84.0	6.30
240	94.9	19.6	94.2	17.3	91.7	12.1	87.3	7.90
360	96.0	25.9	95.7	23.7	92.3	13.0	88.8	8.90
480	96.3	27.0	96.2	26.4	93.3	14.9	90.7	10.7
600	97.4	39.2	97.3	36.5	93.8	16.0	–	–

shows that the η values for the dilute solutions are generally lower than those of the more concentrated one. But at prolonged exposure, i.e. 600 h, the η values for both Ce-inhibitors concentrations increase and become almost identical. It seems that their inhibitive effects become identical, too. However, completely different reasons determine these close values. The higher η values of the more concentrated Ce-solutions (1×10^{-3} M) result from the high inhibitive abilities of the Ce(III) salts. As pointed above this effect is really weak at lower concentrations (5×10^{-5} M) but as the corrosion products exert an additional effect the high η values observed in this case are in fact apparent.

3.2. Superficial morphology

Fig. 4 shows a SEM image of AA2024 specimen after 600 h of exposure to 0.01 M NaCl containing 1×10^{-3} M $Ce(NO_3)_3$.

Two kinds of island-like sediments are distinguished (Fig. 4a). The EDX analysis reveals that the brighter but smaller deposits (designated by "1") have higher cerium concentration – 10.56% (Fig. 4b). It originates from the cerium oxides/hydroxides deposited on the intermetallic S-phase. The larger dark grey deposits designated by "2" contain 50.07% wt. of aluminium and 48.66% wt. of oxygen (Fig. 4c). The composition is similar to that of Al_2O_3 and results from the re-passivation of another kind of pits. Their appearance is attributed to the defects of the oxide film.

Obviously, there are two kinds of pits of completely different etymology. Those of the first kind form on the sites of the metallic surface where the S-phase intermetallics are situated. This kind originates from the intermetallics dissolution. These particles occupy only 3% of the entire metal surface. The other fraction of the metal surface is covered by a native oxide layer which contains various defects. Furthermore, this film has higher electronic conductivity compared to that of pure aluminium [41]. Both, the defects and the enhanced electronic conductivity in the superficial oxide film promote formation of pits of nature differing from that of the pits resulting from the S-phase dissolution. The mechanism of this process is considered in Ref. [42].

The defects of the oxide film and the Cl^- locations enable the proceeding of the following reaction:

$$Al^0 \rightarrow Al^{3+} + 3e^- \quad (9)$$

The aluminium ions migrate towards the surface of the metal/electrolyte interface. They are subsequently hydrolysed to form either soluble hydroxides (Eq. (10)) or solid corrosion product (Eq. (11)):

$$Al^{3+} + H_2O \rightarrow Al(OH)^{2+} + H^+ \quad (10)$$

$$Al^{3+} + 3H_2O \rightarrow Al(OH)_3 + 3H^+ \quad (11)$$

These reactions convert the pitting formation process to "acidic pitting". At the same time, the Cl^- ions penetrate the acidic pits and form dissolved $AlCl_3$ as illustrated in Fig. 5.

Obviously, the composition of the electrolyte inside the "acidic" pits is different from that in the bulk of the corrosive medium. These acidic pits are meta-stable and cannot reach the critical size required for further growth and consequently they re-passivate. Hence, they do not influence the local alkaline corrosion on the S-phase intermetallics. According to Ref. [41], the following equilibrium can establish at the metal surface/corrosive medium interface:

$$Al_2O_3 + 6H^+ + 6Cl^- \leftrightarrow AlCl_3 + 3H_2O \quad (12)$$

Therefore, whether the acidic pits will continue to grow by $AlCl_3$ formation or will re-passivate by Al_2O_3 film formation depends on the medium conditions.

3.3. Impedance measurements

As the impedance measurements enable to distinguish the processes at the electrochemical system interfaces some spectra are recorded after 24, 72, 144, 240, 360 and 600 h of specimens exposure to a model corrosive medium composed of 0.01 M NaCl with the addition of 1×10^{-3} M of the cerium salts studied. Fig. 6 and 7 show the impedance spectra in Nyquist and Bode plots, respectively obtained in case of four different times of exposure.

It is obvious from Fig. 6 that the radius, r, of the capacitive semicircles in the Nyquist plots and the impedance modulus $|Z|$ at $f = 10^{-2}$ Hz for the corresponding Bode plots (Fig. 7) are different for the salts studied although the concentration and the exposure time are identical. These two terms (r and $|Z|$) are used for rough estimation of the inhibitive efficiency of the various inhibitors. Structural impedance modelling is performed for precise quantitative interpretation of the impedance spectra. The selection of the equivalent schemes is done on the ground of the shape of the

Please cite this article in press as: M. Machkova et al., Effect of the anionic part of various Ce(III) salts on the corrosion inhibition efficiency of AA2024 aluminium alloy, Corros. Sci. (2013), http://dx.doi.org/10.1016/j.corsci.2013.01.008

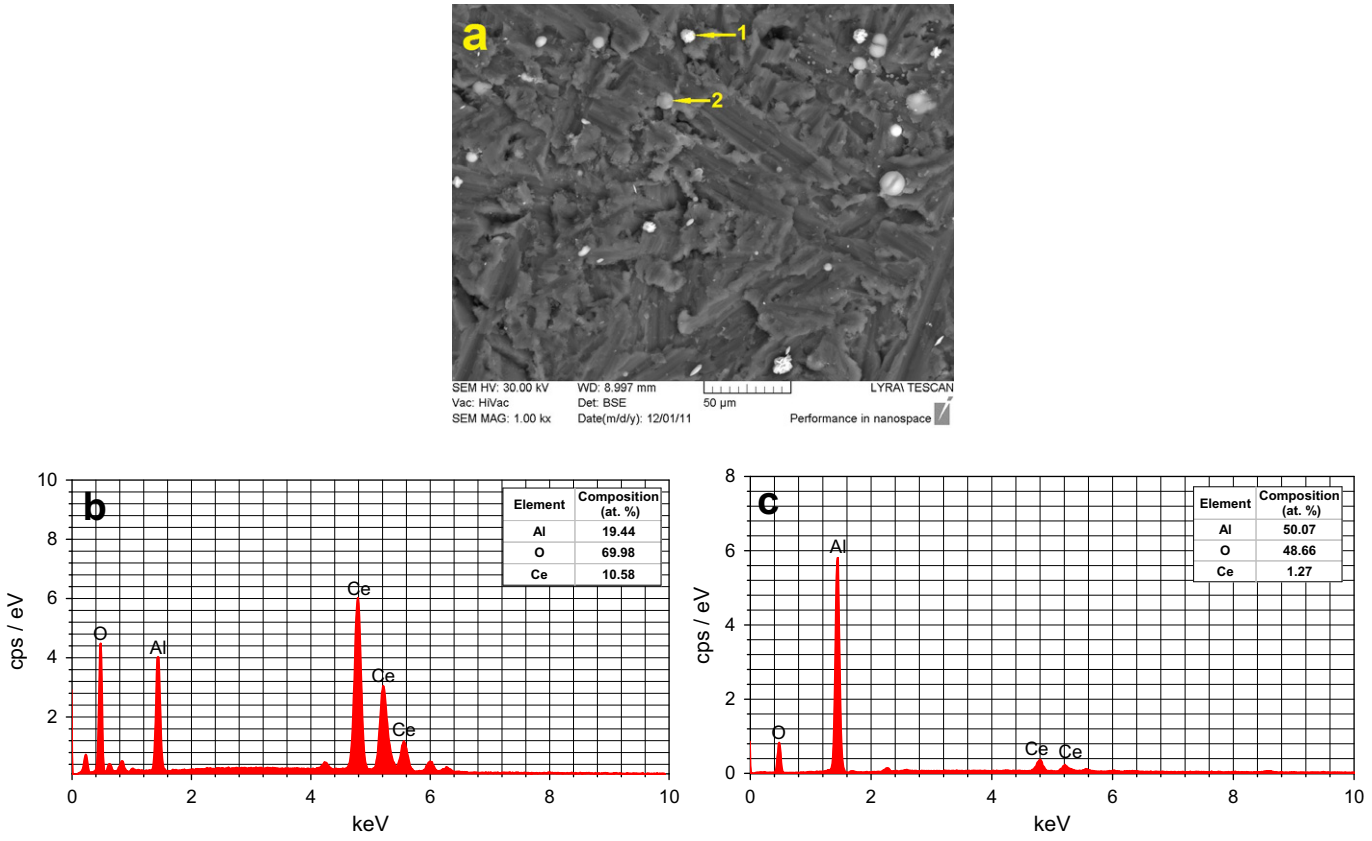

Fig. 4. SEM image (a) and EDS spectra (b and c) of AA2024 specimen, after 600 h of exposition to 0.01 M NaCl solution, with 1×10^{-3} M concentration of $Ce(NO_3)_3$.

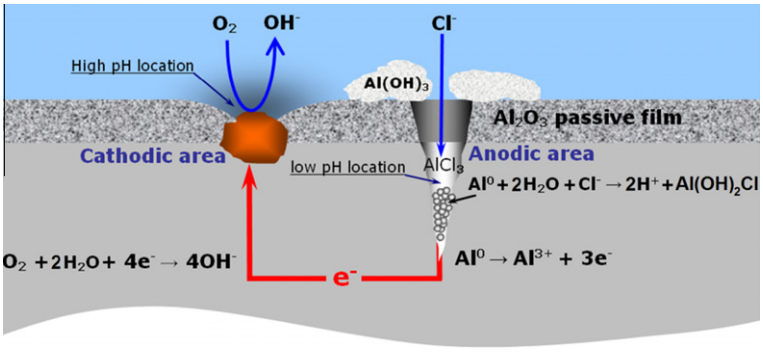

Fig. 5. An illustrative model of acidic pitting formation in the case of AA2024 aluminium alloy corrosion.

experimental impedance spectra. The equivalent circuits used for modelling of the spectra obtained are presented in Fig. 8.

It is seen from Fig. 8a that the complex response of the system is modelled by one time constant $\tau = R_{ct}\ C_{edl}$ that is the response of the metal/electrolyte interface. The time constant $\tau = R_{oxy}\ C_{oxy}$ ascribed to the superficial oxide film is not self standing but is rather overlapped with that of the metal/electrolyte interface. Similar overlaps have been observed for other electrochemical systems [43]. They appear when the capacitances of both time constants have comparable values [44]. Fig. 8b shows the equivalent scheme used for modelling of the impedance spectra in case of $Ce_2(SO_4)_3$. It contains an additive $R_{sl}\ C_{sl}$ unit related to the salt film formed on the surface of the alloy sample. This film consists of aluminium hydroxyl sulphates so that it has low ohmic resistance and weakly expressed barrier ability.

In both equivalent schemes, constant phase elements, Q, are used instead of pure capacitances, C. Their impedance is a frequency dependent term and can be described by the following equation:

$$Q = Y_0^{-1}(j\omega)^{-n} \tag{13}$$

where Y_0 and n are constants independent on the angular frequency ω. For values in the range of $0.8 < n \leqslant 1$, the constant Y_0 has the physical meaning of capacitance. The substitution of C by Q is applicable in cases when the phase shift of the current in respect to the voltage is less than 90°, i.e. when there is a non-ideal capacitor.

The diffusion processes are described by Warburg element (W) which can be expressed as follows:

$$W = \frac{1}{Y_W}(j\omega)^{-1/2} \tag{14}$$

Please cite this article in press as: M. Machkova et al., Effect of the anionic part of various Ce(III) salts on the corrosion inhibition efficiency of AA2024 aluminium alloy, Corros. Sci. (2013), http://dx.doi.org/10.1016/j.corsci.2013.01.008

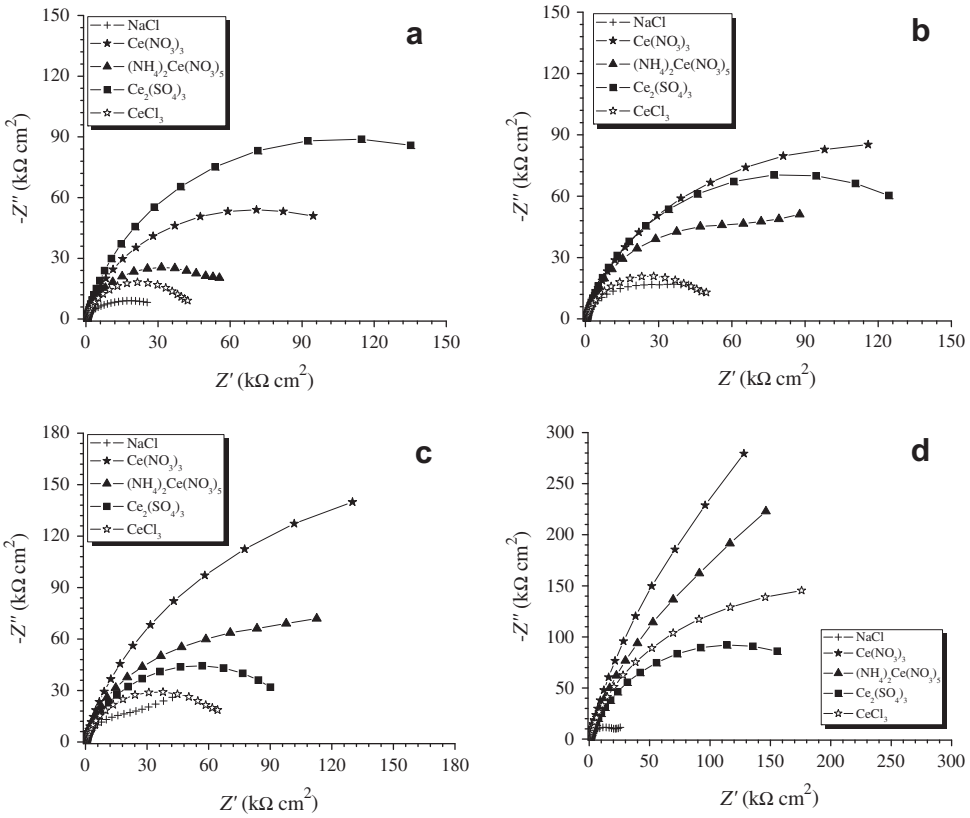

Fig. 6. Impedance spectra in Nyquist plots for samples of the alloy for different times of exposure to model corrosive media, composed by 0.01 M NaCl with 1×10^{-3} M concentration of the respective Ce salts: a – 24 h; b – 72 h; c – 144 h; d – 600 h.

where Y_W is a frequency independent parameter, as well. The inclusion of the Warburg element in the equivalent circuit in Fig. 8a results in remarkable accuracy of the fitting procedures. The lack of whatever sloped (45°) linear dependence between Z' and Z'' in the Nyquist diagrams, typical for the Warburg element, originates from the fact that the entire spectra are shifted to very low frequencies. However, no experiments are carried out at frequencies lower than 10^{-2} Hz, because the determination of a single extra spectral point requires time (in the range of hours) that may not provide the exclusion of any changes in the system's state.

The values of the impedance parameters obtained in impedance spectra modelling (in case of 24 and 240 h of exposure time) are summarised in Table 4.

The data in Table 4 show that the values of the capacitance of the electric double layer are completely reliable and they correspond to the capacitance of a typical metal/solution interface. The table shows the numerical values of the χ^2 criterion which provides to evaluate the measurements accuracy. The values $\chi^2 = 10^{-3}$ and $\chi^2 = 10^{-4}$ show that the modelling performed is almost perfect.

The impedance spectra confirm the results obtained by the polarisation measurements. Fig. 9 juxtaposes graphically the values of R_p obtained by the polarisation measurements and those of R_{ct} determined by the impedance measurements. It is seen that there is concordance between these terms. It is evident that the data-points corresponding to R_p and R_{ct} are ordered in a straight line of a slope of 1 which is further evidence that R_p and R_{ct} have similar values. The calculations show that the average difference between them does not exceed 10%.

The variation of the impedance parameters during the entire exposure of the samples to the corrosive media (from 24 to 600 h) is presented in Figs. 10 and 11. Fig. 10 illustrates the fact that the charge transfer resistance increases during the exposure of the samples, i.e. their inhibitive efficiencies increase. In respect to this parameter, the line of the Ce(III) salts studied is as follows: $Ce(NO_3)_3 > (NH_4)_2Ce(NO_3)_5 > Ce_2(SO_4)_3 > CeCl_3$.

The permanent increase of R_{ct} values can be explained in view of the improvement of the oxide film characteristics resulting from the deposition of Ce-oxides/hydroxides on the less active cathodic areas at the alloy surface as well as from the obstruction of the oxide layer micro-cracks by corrosion products [45].

The unique exclusion from this trend refers to solutions containing $Ce_2(SO_4)_3$. Cerium sulphate appears to be the most efficient inhibitor during the initial 24 h. But then its inhibitive efficiency decreases, and subsequently, after about 140 h, it starts slowly to increase again (even until the 600th hour). This behaviour of Ce sulphate can be attributed to the fact that a salt film is formed on the samples surface. It has weak barrier abilities and cannot provide efficient protection. Its resistance is a several ohms (see Table 4) and is orders of magnitude lower than R_{ct}.

The variation of the electric double layer capacitance at the metal/electrolyte interface with the specimens' exposure time to the model corrosive media containing 1×10^{-3} M of the cerium salts investigated is presented in Fig. 11.

Fig. 11 shows that the capacitance of the electric double layer, C_{edl} (Q_{edl}, respectively) decreases with the exposure time in the solutions of $Ce(NO_3)_3$, $(NH_4)_2Ce(NO_3)_5$, or $CeCl_3$. In accord with the considerations referred to the impedance modelling, C_{edl} includes the value of the capacitance of the superficial oxide layer, C_{oxy}, as well. The observed decrease of C_{edl} can be explained taking into an account that the specific capacitance of a flat capacitor is expressed by:

$$C = \frac{\varepsilon_0 \varepsilon}{d} \quad (15)$$

Please cite this article in press as: M. Machkova et al., Effect of the anionic part of various Ce(III) salts on the corrosion inhibition efficiency of AA2024 aluminium alloy, Corros. Sci. (2013), http://dx.doi.org/10.1016/j.corsci.2013.01.008

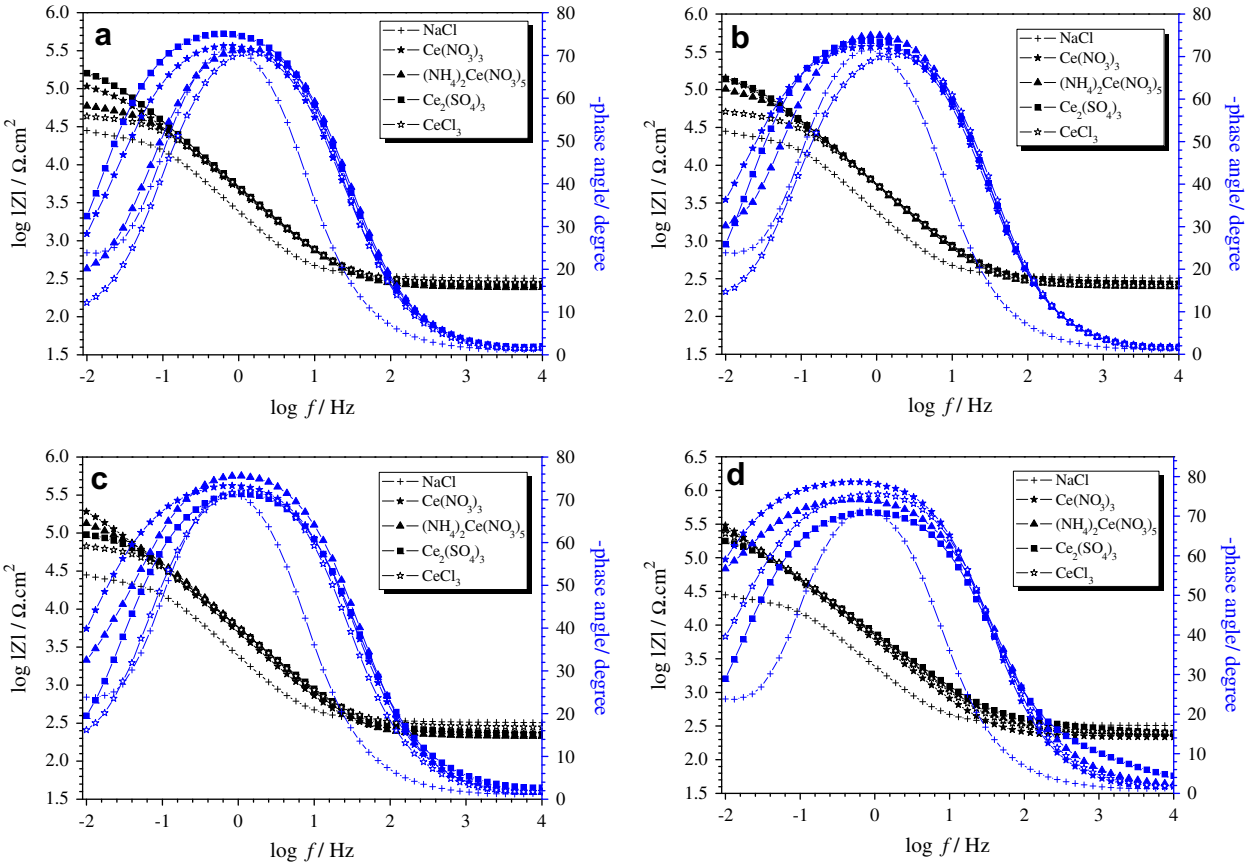

Fig. 7. Impedance spectra in Bode plots for samples of the alloy for different times of exposure to model corrosive media, composed by 0.01 M NaCl with 1×10^{-3} M concentration of the respective Ce salts: (a) 24 h; (b) 72 h; (c) 144 h; (d) 600 h.

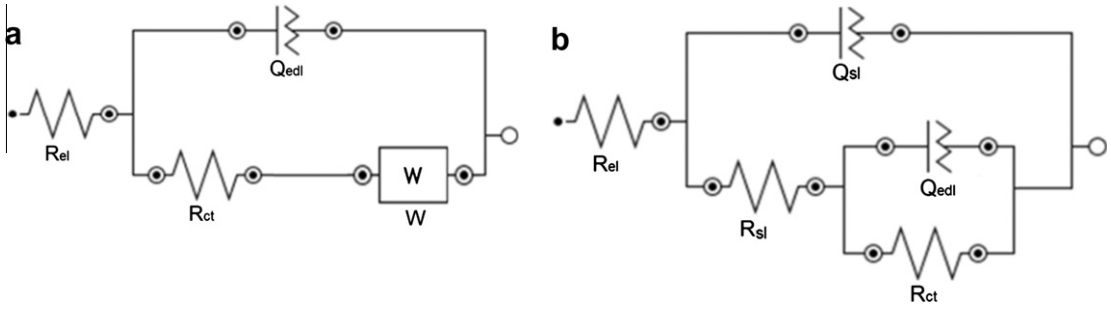

Fig. 8. Equivalent circuits used for structural impedance modelling. R_{el} – electrolyte resistance; R_{ct} – charge transfer resistance; R_{sl} – resistance of the superficial salt layer; Q_{edl} – constant phase element of the double electric layer; Q_{sl} – constant phase element of the superficial salt film and W – Warburg element.

Table 4
Numerical values of the impedance parameters obtained from the impedance modelling procedure.

Fitting parameters	24 h				240 h			
	$Ce(NO_3)_3$	$(NH_4)_2Ce(NO_3)_5$	$Ce_2(SO_4)_3$	$CeCl_3$	$Ce(NO_3)_3$	$(NH_4)_2Ce(NO_3)_5$	$Ce_2(SO_4)_3$	$CeCl_3$
R_{el} (Ω cm^2)	283	245	266	286	270	235	264	268
R_{ct} (kΩ cm^2)	128.1	57.4	216.6	42.4	329	270	181	100.7
Q_{edl} 10^{-4} (s^n Ω^{-1} cm^{-2})	0.44	0.41	0.091	0.36	0.33	0.31	0.18	0.32
n_{edl}	0.86	0.87	0.86	0.88	0.86	0.89	0.84	0.86
R_{sl} (Ω cm^2)	–	–	294	–	–	–	176	–
Q_{sl} 10^{-4}(s^n Ω^{-1} cm^{-2})	–	–	0.30	–	–	–	0.12	–
n_{sl}	–	–	0.88	–	–	–	0.86	–
W 10^{-3}(Ω $s^{-1/2}$ cm^{-2})	0.35	0.36	–	1.0	0.042	0.059	–	0.24
χ^2 10^{-3}	2.6	9.1	0.02	7.3	2.7	10.4	1.8	8.4

Please cite this article in press as: M. Machkova et al., Effect of the anionic part of various Ce(III) salts on the corrosion inhibition efficiency of AA2024 aluminium alloy, Corros. Sci. (2013), http://dx.doi.org/10.1016/j.corsci.2013.01.008

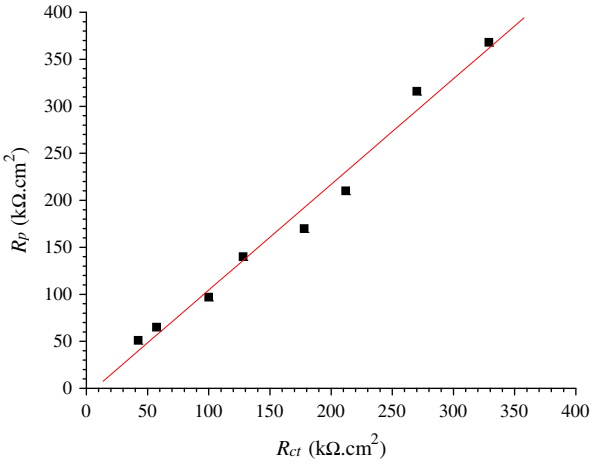

Fig. 9. Graphical juxtaposition of the values of the polarisation resistance R_p acquired by polarisation measurements (Table 2a) with the values charge transfer resistance R_{ct} estimated by the impedance spectra (Table 4).

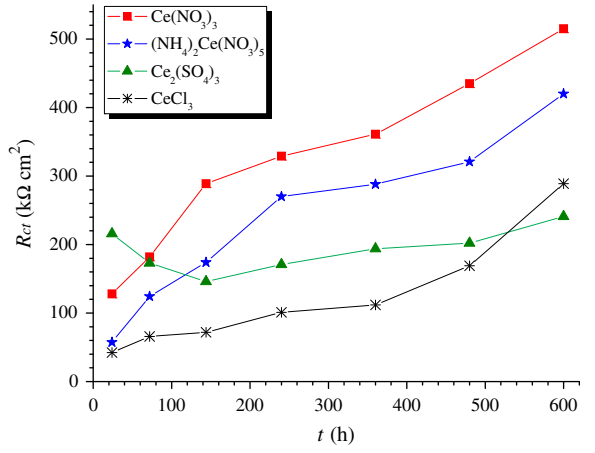

Fig. 10. Development of the charge transfer resistance within the exposure time of the specimens into the model corrosive media with 1×10^{-3} M concentration of different cerium salts.

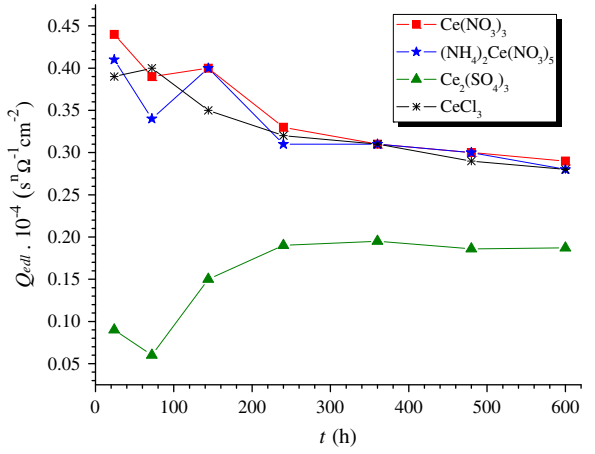

Fig. 11. Evolution of the electric double layer capacitance in metal/electrolyte interface within the exposure time of the specimens into the model corrosive media with 1×10^{-3} M concentration of different cerium salts.

where ε_0 is the electric constant, ε is relative dielectric permeability of the medium, while d is thickness of the dielectric medium. In accordance with Eq. (15), the capacitance decreases because of the increase of the oxide film thickness during the exposure time. The unique exclusion refers to the capacitance of the electric double layer in case of $Ce_2(SO_4)_3$ solutions. It is obvious that after some initial changes, the capacitance remains constant in the entire interval ranging from 250 to 600 h. During this period, the thickness of the oxide film does not increase. It can be explained with the fact that the superficial salt film, although of low resistance, prevents the increase of the oxide layer.

4. Conclusions

The salts of Ce(III) ions reveal different inhibitive efficiencies against the AA2024 corrosion. At lower concentrations of the cerium salts (5×10^{-5} M) in the model corrosive medium, the mechanism of the protective action of all cerium salts studied is identical. It is attributed to the deposition of Ce-hydroxides at the cathodic areas of the metallic surface. At higher concentrations (1×10^{-2} M) $Ce(NO_3)_3$ and $(NH_4)_2Ce(NO_3)_5$ reveal behaviour which differs from that of the other two Ce(III) salts. They act simultaneously as accelerators of the cathodic reactions of the corrosion process and inhibitors of the anodic reaction of alloy dissolution. It is found that NO_3^- ions participate directly in the cathodic reactions of the corrosion process hindering the formation of Cu_2O barrier layer on the re-deposited copper at the sample's surface. The anionic compositional part of the Ce(III) salts studied affects not only the inhibitive efficiency, but the inhibition mechanism as well. It is found that two kinds of pits are formed on the surface. The first one is attributed to the intermetallics inclusions corrosion, whereas the second one refers to the presence of defects in the oxide film. These pits are meta-stable and cannot reach the critical size required for further growth. They re-passivate easily, so that they do not affect the local alkaline corrosion of the S-phase intermetallics.

After extended periods (24–600 h) of exposure of the samples to the corrosive medium the inhibitive efficiency of the solutions containing $Ce(NO_3)_3$, $(NH_4)_2Ce(NO_3)_5$ and $CeCl_3$ increases gradually, whereas that containing $Ce_2(SO_4)_3$ passes through a maximum. In that particular case a salt film is formed on the sample surface. This film has weakly expressed barrier ability, although it hinders the aggressive Cl^- ions access to the substrate surface. The line of the Ce(III) salts studied in respect to their inhibitive efficiency against AA2024 corrosion is as follows: $Ce(NO_3)_3 > (NH_4)_2Ce(NO_3)_5 > Ce_2(SO_4)_3 > CeCl_3$.

Acknowledgments

The authors appreciate the support of this work by the National Science Fund, Bulgaria through Contract DVU No. 02/102. They recognize the exceptionally valuable contribution of Assoc. Prof. Dr. I. Nenov to the development of the experimental procedure used in this study and the mechanistic ideas advanced.

References

[1] T. Kvackaj, R. Bidulský, Aluminium Alloys, Theory and Applications, InTech, Rijeka, 2011.
[2] J.G. Kaufman, Aluminum Alloy Database, in: Knovel portal, updated 2009.
[3] I.J. Polmear, Cast aluminium alloys, in: Light Alloys (Fourth Edition), Butterworth-Heinemann, Oxford, 2005, pp. 205–235.
[4] G.M. Scamans, N. Birbilis, R.G. Buchheit, J.A.R. Editor-in-Chief: Tony (Eds.), Shreir's Corrosion, Elsevier, Oxford,, 2010, pp. 1974–2010.
[5] K.F. Khaled, Corros. Sci. 52 (2010) 2905–2916.
[6] A.M. Abdel-Gaber, E. Khamis, H. Abo-ElDahab, S. Adeel, Mater. Chem. Phys. 109 (2008) 297–305.
[7] R. Sabino, D. Azambuja, R. Gonçalves, J. Solid State Electrochem. 14 (2010) 1255–1260.
[8] J. Bibber, Met. Finish. 96 (1998) 28–31.
[9] M.H.L. Garnaud, Polym. Paint. Col. 174 (1984) 268.

[10] H. Shi, E.-H. Han, F. Liu, Corros. Sci. 53 (2011) 2374–2384.
[11] T.G. Harvey, S.G. Hardin, A.E. Hughes, T.H. Muster, P.A. White, T.A. Markley, P.A. Corrigan, J. Mardel, S.J. Garcia, J.M.C. Mol, A.M. Glenn, Corros. Sci. 53 (2011) 2184–2190.
[12] K.W. Dalzell, Surf. Coat. Aust. 28 (1991) 16.
[13] R.L. Twite, G.P. Bierwagen, Prog. Org. Coat. 33 (1998) 91–100.
[14] M. Bethencourt, F.J. Botana, J.J. Calvino, M. Marcos, M.A. RodrÍguez-Chacón, Corros. Sci. 40 (1998) 1803–1819.
[15] B.R.W. Hinton, D.R. Arnot, N.E. Ryan, Met. Forum 7 (1984) 211–217.
[16] B.R.W. Hinton, D.R. Arnot, N.E. Ryan, Met. Forum 9 (1986) 162–173.
[17] M. Bethencourt, F.J. Botana, M.A. Cauqui, M. Marcos, J.A. Pérez, J.M. Pintado, Ibero-Americano, Corros. Protec. 1 (1995) 321.
[18] A. Aballe, M. Bethencourt, F.J. Botana, M. Marcos, J. Alloys Compd. 323–324 (2001) 855–858.
[19] M.A. Arenas, M. Bethencourt, F.J. Botana, J. de Damborenea, M. Marcos, Corros. Sci. 43 (2001) 157–170.
[20] B. Gu, J. Liu, J. Rare Earths 24 (2006) 89–96.
[21] H. Allachi, F. Chaouket, K. Draoui, J. Alloys Compd. 475 (2009) 300–303.
[22] K.A. Yasakau, M.L. Zheludkevich, M.G.S. Ferreira, J. Electrochem. Soc. 155 (2008) C169–C177.
[23] A.K. Mishra, R. Balasubramaniam, Corros. Sci. 49 (2007) 1027–1044.
[24] B. Davó, J.J. de Damborenea, Electrochim. Acta. 49 (2004) 4957–4965.
[25] N.C. Rosero-Navarro, M. Curioni, R. Bingham, A. Durán, M. Aparicio, R.A. Cottis, G.E. Thompson, Corros. Sci. 52 (2010) 3356–3366.
[26] M.L. Zheludkevich, R. Serra, M.F. Montemor, K.A. Yasakau, I.M.M. Salvado, M.G.S. Ferreira, Electrochim. Acta. 51 (2005) 208–217.
[27] A.K. Bhattamishra, M.K. Banerjee, Zeitschrift fur metallkunde 84 (1993) 734–736.
[28] M. Schem, T. Schmidt, H. Caparrotti, M. Wittmar, M. Veith, In: Eurocorr, Freiburg, Germany, 2007.
[29] E.A. Matter, S. Kozhukharov, M. Machkova, V. Kozhukharov, Mater. Corros. (2012), http://dx.doi.org/10.1002/maco.201106349.
[30] E.A. Matter, S. Kozhukharov, M. Machkova, V. Kozhukharov, Corros. Sci. 62 (2012) 22–33.
[31] M.F. Montemor, A.M. Simões, M.G.S. Ferreira, M.J. Carmezim, Appl. Surf. Sci. 254 (2008) 1806–1814.
[32] A. Decroly, J.P. Petitjean, Surf. Coat. Technol. 194 (2005) 1–9.
[33] M. Bethencourt, F.J. Botana, M.J. Cano, M. Marcos, J.M. Sánchez-Amaya, L. González-Rovira, Corros. Sci. 51 (2009) 518–524.
[34] K.A. Yasakau, M.L. Zheludkevich, S.V. Lamaka, M.G.S. Ferreira, J. Phys. Chem. B 110 (2006) 5515–5528.
[35] N.D. Tomashov, Corrosion and protection of the metals, in (Gov. Ed.) "Nauka", Moskow, 1952, pp. 159.
[36] V. Guillaumin, G. Mankowski, Corros. Sci. 41 (1999) 421–438.
[37] Y. Liu, M.A. Arenas, S.J. Garcia-Vergara, T. Hashimoto, P. Skeldon, G.E. Thompson, H. Habazaki, P. Bailey, T.C.Q. Noakes, Corros. Sci. 50 (2008) 1475–1480.
[38] E.V. Filimonov, A.I. Shcherbakov, Prot. Met. 40 (2004) 280–285.
[39] D. Lau, A.M. Glenn, A.E. Hughes, F.H. Scholes, T.H. Muster, S.G. Hardin, Surf. Coat. Technol. 203 (2009) 2937–2945.
[40] N. Hackerman, R.A. Powers, J. Phys. Chem. 57 (1953) 139.
[41] H. Kaesche (Gov. Ed.), Metallurgy, Moskow, 1984, pp. 219 (in Russian).
[42] K.S. Rao, K.P. Rao, Trans. Indian Inst. Met. 57 (2004) 593–610.
[43] A.K. Mishra, R. Balasubramaniam, Mater. Chem. Phys. 103 (2007) 385–393.
[44] Z. Stoynov, D. Vladikova, Differential Impedance Analysis, in: Marin Drinov Academic (Ed). House, Sofia, 2005, pp. 80.
[45] A. Frignani, F. Zucchi, B. Trabanelli, V. Grassi, Corros. Sci. 48 (2006) 2258–2273.

Please cite this article in press as: M. Machkova et al., Effect of the anionic part of various Ce(III) salts on the corrosion inhibition efficiency of AA2024 aluminium alloy, Corros. Sci. (2013), http://dx.doi.org/10.1016/j.corsci.2013.01.008